Locally Adaptive Nakagami-Based Ultrasound Similarity Measures

Christian Wachinger, Tassilo Klein, Nassir Navab

Computer Aided Medical Procedures (CAMP), Technische Universität München, München, Germany

Abstract

The derivation of statistically optimal similarity measures for intensity-based registration is possible by modeling the underlying image noise distribution. The parameters of these distributions are, however, commonly set heuristically across all images. In this article, we show that the estimation of the parameters on the present images largely improves the registration, which is a consequence of the more accurate characterization of the image noise. More precisely, instead of having constant parameters over the entire image domain, we estimate them on patches, leading to a local adaptation of the similarity measure. While this basic idea of creating locally adaptive metrics is interesting for various fields of application, we present the derivation for ultrasound imaging. The domain of ultrasound is particularly appealing for this approach, due to the inherent contamination with speckle noise. Furthermore, there exist detailed analyses of suitable noise distributions in the literature. We present experiments for applying a bivariate Nakagami distribution that facilitates modeling of several scattering scenarios prominent in medical ultrasound. Depending on the number of scatterers per resolution cell and the presence of coherent structures, different Nakagami parameters are required to obtain a valid approximation of the intensity statistics and to account for distributional locality. Our registration results on radio-frequency ultrasound data confirm the theoretical necessity for a spatial adaptation of similarity metrics.

*Corresponding Author: Christian Wachinger, Boltzmannstr.3, 86574 Garching b. München, Germany; wachinge@in.tum.de, 0049 89 28917077

**Christian Wachinger is currently with the Massachusetts Institute of Technology, Cambridge.

Preprint submitted to Elsevier

Keywords: Ultrasound, Registration, Nakagami, Local Adaptation, Similarity Measure

1. Introduction

Being a crucial component in several fields of application, registration of images is of high interest in medical imaging. Generally, achieving this automatically is impeded by image noise and artifacts. The alignment of ultrasound (US) images is considered to be especially challenging due to the inherent contamination of the images with speckle noise. Clinical applications for ultrasound registration are panorama imaging [1, 2], elastography [3, 4], tracking [5], and motion recovery [6]. The adaptation of similarity measures in ultrasound registration to cope with issues related to noise is an active field of research. A popular approach from speckle tracking is to replace the common assumption of a Gaussian distribution in similarity measures by ultrasound specific noise models. Commonly, a Rayleigh distribution is assumed [6, 7, 8, 9].

In the field of segmentation and classification, research on various distributions for modeling ultrasound scattering has been performed over the last years. We refer to [10] for a recent review. In this respect, it was shown that the commonly applied Rayleigh distribution only models a specific scattering scenario. Alternative distributions were introduced that deal with varying numbers of scatterers per resolution cell and the presence of coherent structures [11]. Especially interesting is the Nakagami distribution, because it allows for modeling a large number of scattering conditions, while being computationally efficient [12]. Adaptation to various noise conditions is achieved by setting the shape and scale parameter of the Nakagami distribution accordingly.

We would like to benefit from the more accurate characterization of speckle statistics of the Nakagami distribution for image registration. This leads to our first major contribution, which is a Nakagami-based similarity measure for the registration of ultrasound envelope data. It is, however, not sufficient to set the Nakagami distribution parameters globally, because they have to be adapted to the local scattering scenario. Our second major contribution is therefore to adapt the similarity measure locally to various scattering scenarios in the image. The focus of this article is on ultrasound registration, however, the local adaptation of similarity measures is of general interest and also applicable to other domains. To the best of the authors

knowledge, this is the first time that the distribution parameters are estimated on the images to adapt the similarity measure.

The organization of the manuscript is at follows. In section 2, we present details about modeling speckle statistics. We provide details about the used radio-frequency ultrasound data and introduce the Nakagami distribution. In section 3, we incorporate the Nakagami distribution in a maximum likelihood framework for image registration. This is followed by the proposal of our novel adaptive similarity measure. Finally, this section is concluded with an elaboration on the estimation of the distribution parameters. In section 4, we evaluate the performance on local block matching and global rigid registration for several ultrasound datasets. The results of multiple random registration studies show the improvement of the devised method.

1.1. Related Work

A large number of articles addresses the registration of ultrasound images [4, 6, 7, 8, 9, 13, 14, 15, 16, 17, 18, 19, 20, 21]. Typical application areas are (i) motion measurements in echocardiography for detecting and characterizing abnormalities, (ii) breast deformation analysis to assess the elastic properties of tissues, (iii) assessment of tissue strain with elastography, and (iv) multi-view compounding. In [7], likelihood functions are presented assuming a multiplicative Rayleigh noise. This is further extended in [6], assuming that both, the moving and the fixed image, are affected by multiplicative speckle noise. Moreover, the log-compression is incorporated in the imaging model to achieve better results on B-mode data. These similarity metrics are successfully applied in [8, 9] for motion estimation with a block matching approach. In [4], block matching with normalized cross-correlation (NCC) is performed for flow and elasticity imaging. In [13, 16], a block matching approach is applied to improve the quality of compounded images. While Krücker *et al.* [13] evaluate several similarity measures, with the conclusion that sum of squared differences (SSD) is better suited for low noise levels, Poon and Rohling [16] focus on NCC. Myronenko *et al.* [21] presented similarity measures based on the bivariate Rayleigh and Nakagami distributions. Contrarily to previous approaches, they do not work on B-mode images but on log-compressed envelope data [21]. This is important because B-mode images have corrupted speckle statistics due to applied non-linear transformations, as will be discussed in more detail later on. For our own approach, we directly work on the envelope data. Common to all the presented methods is that the parameters of the distributions are set heuristically on a

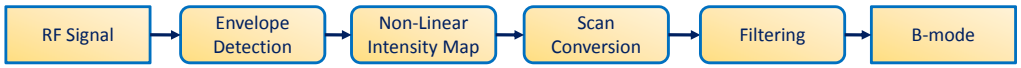

Figure 1: Example ultrasound processing pipeline for RF to B-mode conversion.

global basis, which is at odds with the underlying local data variation. For instance, the variance of the Rayleigh distribution is set to $2/\pi$ in [6], or the shape and correlation parameters are set to $m = 0.5, \rho = 0.8$ in [21]. In the proposed method, we exactly address this issue by locally estimating these parameters on the images.

Next to ultrasound specific approaches, we also want to mention related work in terms of general registration. A typical situation that challenges the application of mutual information is the registration of images, which contain high intensity non-uniformity due to the bias field. Approaches that address this issue try to estimate the joint density in local regions or do a combination of local and global estimation [22, 23]. This local adaptation is different to our contribution, because no noise estimates are performed. Recently, learning-based similarity measure were proposed for multi-modal registration [24, 25]. Supervised learning is performed on previously registered data to learn an appropriate similarity function. The necessity of having access to correctly aligned data for training is, however, a major drawback of these methods. The adaptation of the distribution parameters in our approach could be regarded as learning, with the learning being performed on the actual images.

2. Background on Ultrasound Data Statistics

2.1. Radio-frequency Data

The ultrasound data conventionally worked on is referred to as B-mode. In order to get such an image, the raw analog-to-digital converted radio-frequency (RF) data measured by the transducer undergoes several processing steps (see figure 1). First, an envelope detection (e.g. Hilbert transform) is performed in order to remove high frequency oscillations, while keeping the outline of the original signal. This is followed by the application of a non-linear intensity map (log-compression) to reduce the dynamic range of the data. At the final stage of the pipeline, several proprietary image filters specific for manufacturers of ultrasound machines are applied. Depending on the transducer geometry, the correct geometric placement of the scan lines

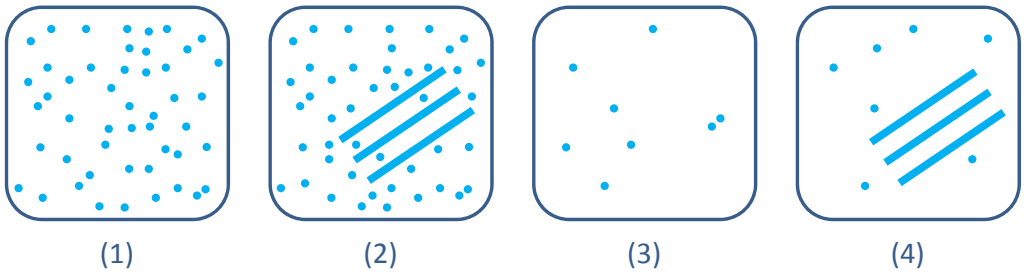

Figure 2: Various scattering scenarios per resolution cell. (1) Larger number of scatters (2) with coherent structure. (3) Small number of scatters (4) with coherent structure.

is achieved with a scan-conversion. It transforms the data into Cartesian coordinate frame entailing interpolation to form an image without gaps on a regular grid. However, as the filtering is mainly meant to optimize data for the human eye, the data flow through the pipeline incurs a loss of information, which is naturally detrimental for machine processing.

Recent work suggests a benefit in using RF data for statistical processing. Shankar [12] showed that the envelope of the RF signal can be modeled by the Nakagami distribution and its parameters are suitable for tissue classification [26]. In [27], a variant of the previous classification method is suggested, using a small window kernel regression to guarantee locality. In [28], an ultrasound specific auto-model is proposed by embedding the Nakagami distribution into a Markov random field (MRF) facilitating the classification of cancerous breast tissue. Similarly, Klein *et al*. [29] developed a MRF-based feature descriptor for tissue classification and image registration.

We apply a recently proposed method for the envelope detection of RF data [30] based on the 2D analytic signal [31]. This estimates the envelope of the signal in 2D instead of 1D. It was demonstrated that the incorporation of lateral information leads to a more robust estimation of the local amplitude from ultrasound RF data. Moreover, the extracted envelope bears superior statistical properties, as evaluated with goodness-of-fit tests to Nakagami distributions [30]. Since we want to accurately model the statistical properties of the envelope data in the derived likelihood functions, the calculation of the 2D analytic signal for demodulation is advantageous for our application.

2.2. Statistical Model

A multitude of distributions were proposed for modeling ultrasound envelope statistics, among them there is Rayleigh [32], Rician [33], pre-Rician K [34], generalized K [35], homodyned K [36], as well as Rician Inverse of the Gaussian [37]. Some of them are specific for certain speckle assumptions whereas others are able to model various scenarios. We illustrate four different scattering scenarios in figure 2. For a large number of scatterers, see figure 2 (1), the Rayleigh distribution presents a good approximation. In combination with a coherent component, the Rician distribution is well suited [38], as illustrated in (2). For a small number of scatterers, the K distribution and homodyned K distribution, depending on whether a coherent component is present, are proposed [36], depicted in (3) and (4), respectively. Due to their inherent complexity, the practical applicability of these distributions is often limited. Simpler but nonetheless extremely versatile, the Nakagami distribution [39] was proposed, admitting an explicit analytical expression. In particular, by varying the shape parameter of the Nakagami distribution, it is possible to emulate other distributions such as Rayleigh, Rician or homodyned K-distribution [40, 10]. It was shown to accurately model backscatter characteristics of US envelope [12] data and is used in various applications such as segmentation and classification, see [41, 26] and references therein.

The Nakagami distribution $\mathcal{N}(x \mid m, \omega)$ belongs to the exponential family and requires the specification of two parameters, m and ω, determining shape and scale, respectively

$$\mathcal{N}(x \mid m, \omega) = \frac{2m^m x^{2m-1}}{\Gamma(m)\omega^m} \exp\left(-\frac{m}{\omega}x^2\right), \forall x \in \mathbb{R}_+. \tag{1}$$

In figure 3, we show the histogram of two regions of the ultrasound image together with the corresponding Nakagami MLE fit. The Nakagami parameters estimated on the same RF image are visualized in figure 4. The large variation of the distribution parameters highlights the necessity of spatial adaptation of noise models to accommodate for the speckle locality.

Imaging a static scene several times, the same speckle occurs in the data [42]. Consequently, speckle is different to other types of noises, such as electrical noise, which is entirely random. Generally speaking, speckle occurs at structures that are rough with respect to the scale of the sound wavelength λ (approx. in the range $0.1 \leq \lambda \leq 1.0$ mm). In medical ultrasound, microscopic inhomogeneities, due to the nature of tissue are responsible for characteristic speckle. Given that different tissue exhibit characteristic spatial

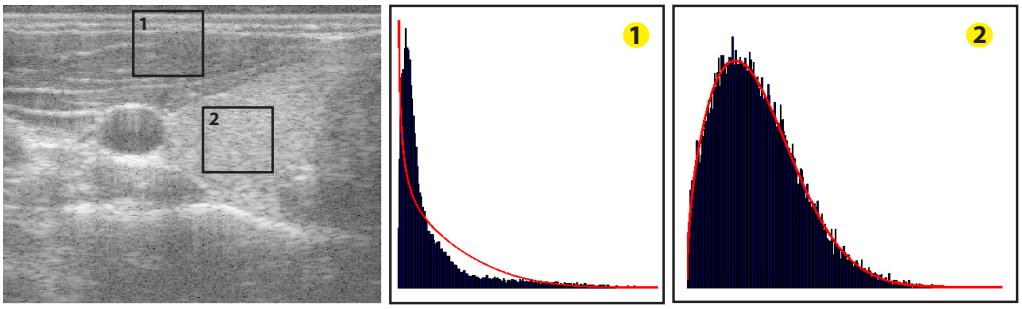

Figure 3: Left: Ultrasound image with two example regions. Middle and right: histograms of the regions together with Nakagami MLE fits (red).

arrangement and size of particles responsible for speckle, texture modeling has been proposed for tasks such as classification or registration [28, 41, 29].

3. Maximum Likelihood Ultrasound Registration

Considering ultrasound envelope images I and J together with the transformation T, registration is formulated as maximum likelihood estimation [43, 44] by

$$\hat{T} = \arg\max_{T} \log p(I \mid J, T, \varepsilon) \tag{2}$$

with $\hat{T}$ the estimated transformation and noise ε. For the derivation of SSD, correlation ratio, or mutual information, an additive Gaussian noise is incorporated in the deduction [44].

3.1. Ultrasound Likelihood Functions

In the following, we present an overview of ultrasound similarity measures proposed in the literature and derive a new locally adaptive Nakagami-based metric. We list several imaging models and denote them with the initials of the authors, prevailing in the literature.

SK_1: Multiplicative Rayleigh Noise

In [7], an imaging model based on a multiplicative Rayleigh noise is presented

$$I = J \cdot \varepsilon \tag{3}$$

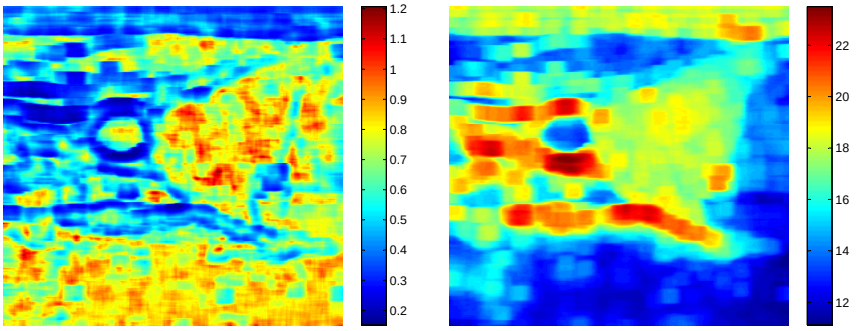

(a) m map (b) ω map

Figure 4: Illustration of Nakagami MLE parameters shape m and scale ω, calculated densely for one image of a human neck.

with ε Rayleigh distributed. This noise model considers only one image to be degraded by noise, while the other one has to be noiseless. Knowing the distribution $p(\varepsilon)$, we have to find the distribution for the likelihood $p(I \mid J, T)$. Assuming that we know the distribution of a random variable x and we want to calculate the distribution of a random variable y, with both being related by the function g, so $y = g(x)$. The fundamental theorem [45, p.93] states that the distribution of the random variable y is calculated with

$$p(y) = \frac{p(x)}{|g'(x)|}. \tag{4}$$

In our case, we set $g(x) = x \cdot J$ and obtain $\frac{dg(x)}{dx} = J$ so that

$$p(I \mid J, T) = \frac{1}{J} \cdot p(\varepsilon). \tag{5}$$

Setting the variance of the Rayleigh distribution to $\frac{2}{\pi}$ leads to the log-likelihood function of SK_1

$$\log p(I \mid J, T) = \log \frac{1}{J} \cdot p\left(\frac{I}{J}\right) \tag{6}$$

$$\approx \log\left(\frac{I}{J^2}\right) - \frac{\pi}{4}\frac{I^2}{J^2}. \tag{7}$$

A second noise model is proposed in [7] with a signal dependent Gaußian noise, not further considered here.

CD_1: Division of Rayleigh Noises

A more realistic and refined model is proposed in [6], assuming that each image is contaminated by a multiplicative Rayleigh noise ε_1 and ε_2, respectively. Considering the underlying, noise-free scene S, the imaging model is formulated as $I = S \cdot \varepsilon_1$ and $J = S \cdot \varepsilon_2$, leading to

$$I = J \cdot \frac{\varepsilon_1}{\varepsilon_2} = J \cdot \eta \tag{8}$$

with the division of probabilities $\eta = \frac{\varepsilon_1}{\varepsilon_2}$. The distribution of the divisional noise $p(\eta)$ is calculated with [45, p.138]

$$p(\eta) = \int_{-\infty}^{\infty} \varepsilon_2 \cdot p(\eta\varepsilon_2, \varepsilon_2)\, \mathrm{d}\varepsilon_2. \tag{9}$$

Considering the noise in the images to be independent

$$p(\varepsilon_1, \varepsilon_2) = p(\varepsilon_1)p(\varepsilon_2) \tag{10}$$

, of equal variance, and Rayleigh distributed, the integration results in

$$p(\eta) = \frac{2 \cdot \eta}{(\eta^2 + 1)^2}. \tag{11}$$

Knowing the distribution $p(\eta)$, we have to find the distribution for the likelihood $P(I \mid J, T)$. This is obtained with the fundamental theorem [45, p.93], setting $g(x) = x \cdot J$, and leading with the derivative $\frac{dg(x)}{dx} = J$ to

$$p(I \mid J, T) = \frac{1}{J} p(\eta) = \frac{1}{J} \int_{-\infty}^{\infty} \varepsilon_2 \cdot p(\eta\varepsilon_2, \varepsilon_2)\, \mathrm{d}\varepsilon_2. \tag{12}$$

The log-likelihood function of CD_1 is

$$\begin{aligned} \log p(I \mid J, T) &= \log \frac{1}{J} \cdot p\left(\frac{I}{J}\right) && (13) \\ &= \log \frac{1}{J} \frac{2 \cdot \frac{I}{J}}{\left(\left(\frac{I}{J}\right)^2 + 1\right)^2} && (14) \\ &\approx \log I - 2 \log J - 2 \log \left[\left(\frac{I}{J}\right)^2 + 1\right]. && (15) \end{aligned}$$

CD_2: Logarithm of Division of Rayleigh Noises

The second model in [6] considers besides the noise contamination of both images also the log-compressed nature of ultrasound images

$$\log I = \log(J \cdot \eta) = \log J + \log \eta. \tag{16}$$

With setting $\tilde{I} = \log I$ and $\tilde{J} = \log J$

$$\eta = \exp(\tilde{I} - \tilde{J}). \tag{17}$$

The likelihood function, applying the fundamental theorem again, but this time with respect to the log-compressed images, is

$$p(\tilde{I} \mid \tilde{J}, T) = \eta \cdot p(\eta). \tag{18}$$

This is obtained with $g(\eta) = \log J + \log \eta$ and the derivative $g'(\eta) = \frac{1}{\eta}$. The log-likelihood function for CD_2 is

$$\begin{aligned}
\log p(\tilde{I} \mid \tilde{J}, T) &= \log \frac{\exp(\tilde{I})}{\exp(\tilde{J})} \cdot p(\exp(\tilde{I} - \tilde{J})) && (19)\\
&= \log \frac{\exp(\tilde{I})}{\exp(\tilde{J})} \cdot \frac{2 \cdot \exp(\tilde{I} - \tilde{J})}{\left[\exp(\tilde{I} - \tilde{J})^2 + 1\right]^2} && (20)\\
&= \log \frac{2 \cdot \exp(2(\tilde{I} - \tilde{J}))}{\left[\exp(2(\tilde{I} - \tilde{J})) + 1\right]^2} && (21)\\
&\approx \tilde{I} - \tilde{J} - \log[\exp(2(\tilde{I} - \tilde{J})) + 1]. && (22)
\end{aligned}$$

The application of the presented ultrasound specific likelihood terms for simultaneous registration is described in [46]. Working with B-mode images, we achieved a superior performance with CD_2 than with SSD and NCC.

3.2. Bivariate Nakagami

In this section, we present the proposed similarity measure based on the Nakagami distribution. As explained in section 2, the Nakagami distribution is more appropriate for modeling speckle statistics in ultrasound than the Rayleigh distribution, which is used in the likelihood functions that we have discussed in section 3.1. For equation (12), a bivariate distribution is

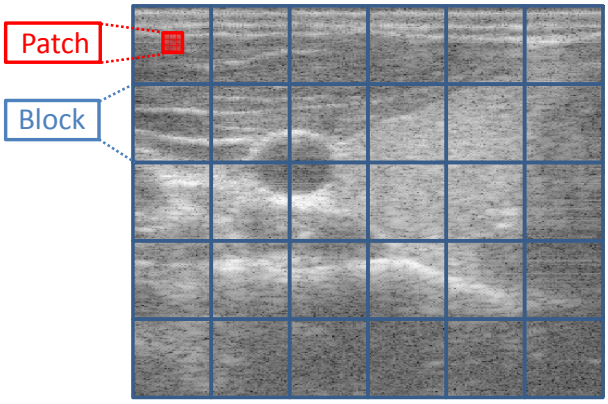

Figure 5: Illustration of the subdivision of the image domain into blocks and patches.

required, if no assumptions about independence are incorporated. Such assumptions are applied for the derivation of CD_1 and CD_2, see equation (10), in conjunction with Rayleigh distributions. Since speckle is due to physical interaction of the beam with the tissue, the same speckle pattern appear under constant acquisition conditions. In modern ultrasound systems with high frame rates and for acquisitions from the same viewing-angle, it is therefore reasonable to assume the random variables ε_1 and ε_2 to be correlated [42]. The bivariate Nakagami distribution is [21]

$$p(\varepsilon_1, \varepsilon_2) = \frac{2^{1-m} m^{m+1} (\varepsilon_1 \varepsilon_2)^m}{\sigma^{2(m+1)} (1-\rho) \rho^{(m-1)/2} \Gamma(m)} e^{-\frac{m(\varepsilon_1^2+\varepsilon_2^2)}{2(1-\rho)\sigma^2}} I_{m-1}\left(-\frac{m\sqrt{\rho}\varepsilon_1\varepsilon_2}{(1-\rho)\sigma^2}\right) \quad (23)$$

with ρ being a squared correlation coefficient, I_{m-1} is a modified Bessel function of the first kind of order $m-1$, and the distribution widths σ^2 are equal. Incorporating the bivariate Nakagami in the conditional density in equation (12) leads to

$$p(I|J,T) = \frac{1}{J} \int_{-\infty}^{\infty} \varepsilon_2 \cdot p(\eta\varepsilon_2, \varepsilon_2)\, \mathrm{d}\varepsilon_2 \quad (24)$$

$$= \frac{1}{J} 2(1-\rho)^m \frac{\Gamma(2m)}{\Gamma(m)^2} \frac{\eta^{2m-1}}{(\eta^2+1)^{2m}} \left(1 - \frac{4\rho\eta^2}{(\eta^2+1)^2}\right)^{-\frac{2m+1}{2}} \quad (25)$$

$$= \frac{1}{J} \frac{2(1-\rho)^m}{\beta(m)} \cdot \frac{1}{\eta} \cdot \frac{\eta^{2m}}{(\eta^2+1)^{2m}} \cdot \left(1 - \frac{4\rho\eta^2}{(\eta^2+1)^2}\right)^{-\frac{2m+1}{2}} \quad (26)$$

with $\beta(m) = \frac{\Gamma(m)^2}{\Gamma(2m)}$. More details on the deduction, however, assuming log-compressed envelope data and therefore a different imaging model, are presented in [47]. Finally, computing the log-likelihood yields the Nakagami-based similarity measure

$$\begin{aligned}
&\log p(I|J,T) \\
&= -\log J + \log \frac{2(1-\rho)^m}{\beta(m)} - \log \eta + 2m \log \left(\frac{\eta}{\eta^2+1} \right) - \frac{2m+1}{2} \log \left(1 - \frac{4\rho\eta^2}{(\eta^2+1)^2} \right) \\
&= -\log J - \log \left(\frac{I}{J} \right) + 2m \log \left(\frac{\left(\frac{I}{J}\right)}{\left(\frac{I}{J}\right)^2+1} \right) - \frac{2m+1}{2} \log \left(1 - \frac{4\rho \left(\frac{I}{J}\right)^2}{(\left(\frac{I}{J}\right)^2+1)^2} \right).
\end{aligned} \tag{27}$$

3.3. Parameter estimation

We mentioned previously that the Nakagami distribution can characterize different scattering scenarios when setting the distribution parameters appropriately. In this part, we describe how we instantiate the bivariate Nakagami model in each iteration of the similarity computation. Specifically, this requires the specification of a shape parameter m as well as a correlation coefficient ρ, see equation (27). Considering the need for high locality, the patch size has to be kept at minimum. However, this sparsity constraint is detrimental for the computation of the m parameter of the bivariate Nakagami distribution. Additionally, because of the high frequency of this similarity computation, complexity has to be kept at bare minimum. Therefore, we decided to use a fast approximation scheme. The distribution parameters are calculated separately for the moving (m_I, ω_I) and the fixed patches (m_J, ω_J) with maximum likelihood estimation (MLE). Then, given the individual MLE parameters, the joint shape parameter m of the bivariate Nakagami is approximated by $(m_I + m_J)/2$.
For computing the correlation coefficient ρ for the bivariate Nakagami, probably the most obvious way is to directly use the corresponding intensities of the patches. However, due to the noise-susceptibility of ultrasound, a probabilistic correlation score was chosen in order to increase the overall reliability. In this respect, we employ the Bhattacharyya coefficient (BC)

$$BC(p,q) = \int \sqrt{p(x)q(x)}\, dx \tag{28}$$

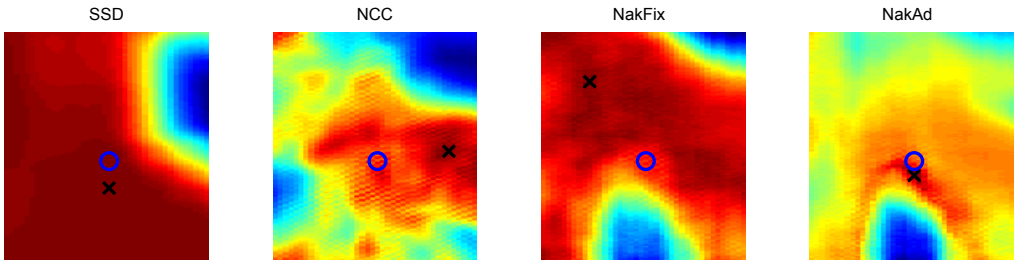

Figure 6: Similarity plots for various measures. Blue circle: correct alignment, black cross: similarity maximum. X axis indicates x-translation from -20 to +20 pixels and Y axis indicates y-translation from -80 to +80 pixels.

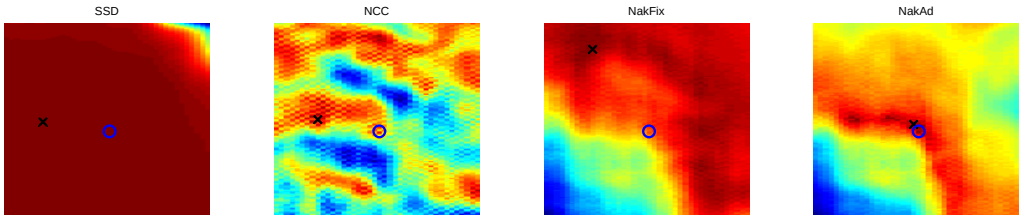

Figure 7: Similarity plots for various measures. Blue circle: correct alignment, black cross: similarity maximum. X axis indicates x-translation from -20 to +20 pixels and Y axis indicates y-translation from -80 to +80 pixels.

with $0 \leq BC \leq 1$, which is a measure of the relative overlap between two probability distributions p and q. In our case, the distributions correspond to the Nakagami MLE estimates of the moving and the fixed image, respectively.

4. Experiments

For our experiments we use a clinical ultrasound system from Ultrasonix (Richmond, Canada). All acquisitions are performed with a linear transducer at 3.3 MHz. The RF data is sampled with 40 MHz and is readily accessible from the system. Depending on the depth setting, the images have a resolution between 1157 and 2080 pixels in axial, and 256 pixels in lateral direction. The images were acquired from the human neck on four healthy volunteers in the age range of 25 to 35. Each dataset consists of a moving and a fixed image.

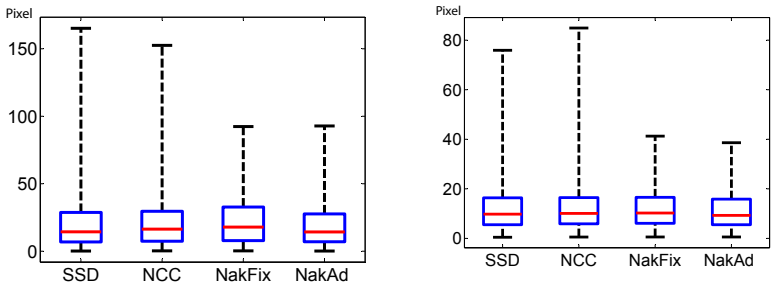

(a) Dataset 1

(b) Dataset 2

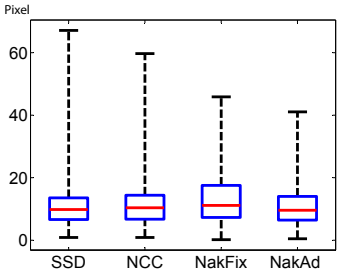

(c) Dataset 3

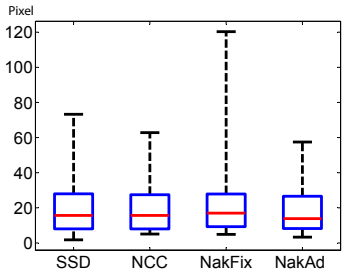

(d) Dataset 4

Figure 8: Boxplots of errors from random registration study for block matching.

We perform block matching on 100 blocks in the images, which are equally distributed across the image. This is schematically illustrated in figure 5. For each block, we have the coordinates from a manual alignment, serving as ground truth data. We compare SSD and NCC with the similarity measure presented in equation (27). Once we use heuristic values for the distribution parameters, referred to as NakFix, and once we estimate them on the images, referred to as NakAd. For the heuristic case, we choose the parameters used in [21] $m = 0.5$ and $\rho = 0.8$. NakFix is therefore the analogon of the similarity measure presented in [21] for not log-compressed envelope data.

To compare the different similarity measures, we extract a patch of 91×11 pixels in the moving image and shift it over the block in the fixed image. The distribution parameters are estimated on these patches. The patch size is a tradeoff between sufficient statistics for parameter estimation and the detection of fine grained deformations. We illustrate similarity plots for two different blocks in figures 6 and 7. In both cases, SSD and NCC are not able

Dataset	SSD	NCC	NakFix	NakAd
Dataset 1	9.3	9.9	10.4	**9.1**
Dataset 2	9.8	10.1	10.2	**9.2**
Dataset 3	9.9	10.4	11.1	**9.5**
Dataset 4	15.7	15.7	17.0	**13.8**

Table 1: Median errors of random registration study for various datasets and similarity metrics.

to correctly indicate the correct alignment. Moreover, the similarity plot of NCC shows several local minima. Also the maximum of NakFix is far off the correct alignment. Interestingly, the adaptation of the parameters, as it is done in NakAd, significantly changed the similarity function, leading to good results in this case.

The similarity plots provide a first impression of the performance, which we further evaluate by performing block matching. As discussed in section 1.1, block matching is commonly applied in ultrasound registration. We extract patches from the moving image and try to find the corresponding patch in the fixed image. For each image, this is done for one patch per block, so on 100 patches. Since we know the alignment of the blocks, we can calculate the Mahalanobis distance with respect to the ground truth position, serving as error measure. We select the Mahalanobis distance to compensate for the significantly higher resolution in axial direction. To be able to perform statistics on the results of the registration, we perform a random registration study. For this we randomly displace the patch 100 times from the ground truth position, with maximal initial deviation of ± 40 pixels in axial and ± 10 pixels in lateral direction. The errors over all patches and all runs are shown in the boxplots in figure 8 for 4 datasets. We list the median errors in table 1. We observe that the median, the box, and the whiskers are lowest for NakAd in all cases. The performance of SSD and NCC is comparable, with slight advantages for NCC with respect to the whiskers. The performance of NakFix for datasets 1 - 3 is slightly worse than NakAd. For dataset 4, NakFix is not leading to good results.

In addition to the analysis of the presented similarity measure for block matching, we also perform experiments for global rigid registration. Therefore, the image is separated into blocks, as already discussed previously. This time, we estimate the parameters for each block and evaluate the simi-

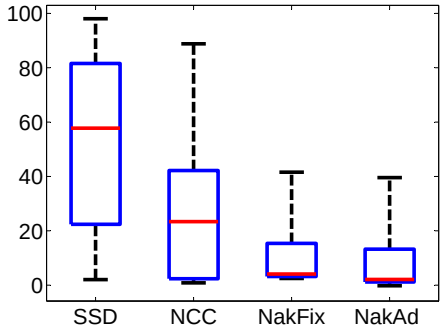

Figure 9: Boxplot of errors from rigid registration study.

larity measure on the block. Accumulating the similarity estimates from all blocks leads to the global similarity estimate. We also perform a random registration study with 100 runs and initial deviations up to ± 240 pixels in axial and ± 70 pixels in lateral direction. The results are shown in figure 9. The median errors are SSD: 57.8, NCC: 23.4, NakFix: 4.1, and NackAd: 2.1. NCC performs better than SSD, but the best results are obtained for the Nakagami-based similarity measures, with the proposed adaptive version outperforming the fixed version.

5. Conclusion

The major contributions of the article are: (i) the introduction of a similarity measure based on the bivariate Nakagami distribution for the registration of envelope ultrasound data, and (ii) the local adaptation of the similarity measure by estimating the distribution parameters on the ultrasound images. As discussed in the article, the adaptation of the similarity measure to various scattering scenarios is necessary to model the noise correctly, and therefore to perform a more appropriate similarity estimation. Experiments are performed on ultrasound RF data. The results from block matching indicate the improvement of incorporating the Nakagami distribution and the necessity of locally adapting the parameters. Moreover, a clear improvement of the proposed similarity measures is shown for the case of global rigid registration.

6. Acknowledgment

The work was partly funded by the European Commission. We are grateful to Mattias Hansson for helping with the experiments and active discussions.

References

[1] W. Henrich, A. Schmider, S. Kjos, B. Tutschek, J. W. Dudenhausen, Advantages of and applications for extended field-of-view ultrasound in obstetrics, Archives of Gynecology and Obstetrics V268 (2003) 121–127.

[2] C. Wachinger, W. Wein, N. Navab, Registration strategies and similarity measures for three-dimensional ultrasound mosaicing, Academic Radiology 15 (2008) 1404–1415.

[3] S. Salcudean, D. French, S. Bachmann, R. Zahiri-Azar, X. Wen, W. Morris, Viscoelasticity modeling of the prostate region using vibroelastography, Medical Image Computing and Computer-Assisted Intervention (2006) 389–396.

[4] A. Basarab, W. Aoudi, H. Liebgott, D. Vray, P. Delachartre, Parametric deformable block matching for ultrasound imaging, in: Image Processing (ICIP). IEEE International Conference on, Vol. 2, 2007, pp. II –429 –II –432.

[5] A. H. Gee, R. J. Housden, P. Hassenpflug, G. M. Treece, R. W. Prager, Sensorless freehand 3d ultrasound in real tissue: Speckle decorrelation without fully developed speckle, Medical Image Analysis 10 (2) (2006) 137 – 149. doi:DOI: 10.1016/j.media.2005.08.001.

[6] B. Cohen, I. Dinstein, New maximum likelihood motion estimation schemes for noisy ultrasound images, Pattern Recognition 35 (2) (2002) 455–463.

[7] M. Strintzis, I. Kokkinidis, Maximum likelihood motion estimation in ultrasound image sequences, Signal Processing Letters, IEEE 4 (6) (1997) 156–157.

[8] D. Boukerroui, J. Noble, M. Brady, Velocity estimation in ultrasound images: a block matching approach, Inf Process Med Imaging 18 (2003) 586–98.

[9] J. Revell, M. Mirmehdi, D. McNally, Combined ultrasound speckle pattern similarity measures, in: Medical Image Understanding and Analysis, BMVA Press, 2004, pp. 149–153.

[10] F. Destrempes, G. Cloutier, A Critical Review and Uniformized Representation of Statistical Distributions Modeling the Ultrasound Echo Envelope, Ultrasound in medicine & biology 36 (7) (2010) 1037–1051.

[11] J. Goodman, Speckle phenomena in optics: theory and applications, Roberts & Co, 2006.

[12] P. M. Shankar, A general statistical model for ultrasonic scattering from tissues, IEEE Trans Ultrason Ferroelectr Freq Control 47 (3) (2000) 339–343.

[13] J. Krucker, G. LeCarpentier, J. Fowlkes, P. Carson, Rapid elastic image registration for 3-d ultrasound, IEEE Transactions on Medical Imaging 21 (11) (2002) 1384–1394.

[14] G. Xiao, J. Brady, J. Noble, M. Burcher, R. English, Nonrigid registration of 3-D free-hand ultrasound images of the breast, Medical Imaging, IEEE Transactions on 21 (4) (2002) 405–412.

[15] D. Zikic, W. Wein, A. Khamene, D.-A. Clevert, N. Navab, Fast deformable registration of 3d-ultrasound using a variational approach, Medical Image Computing and Computer-Assisted Intervention (MICCAI) 4190 (2006) 915–923. doi:10.1007/11866565.

[16] T. Poon, R. Rohling, Three-dimensional extended field-of-view ultrasound, Ultrasound in Medicine and Biology 32 (3) (2005) 357–369.

[17] C. Wachinger, W. Wein, N. Navab, Three-dimensional ultrasound mosaicing, in: International Conference on Medical Image Computing and Computer-Assisted Intervention (MICCAI), Brisbane, Australia, 2007, pp. 327–335.

[18] V. Grau, H. Becher, J. Noble, Registration of multiview real-time 3-d echocardiographic sequences, Medical Imaging, IEEE Transactions on 26 (9) (Sept. 2007) 1154–1165. doi:10.1109/TMI.2007.903568.

[19] A. Elen, H. F. Choi, D. Loeckx, H. Gao, P. Claus, P. Suetens, F. Maes, J. D'hooge, Three-dimensional cardiac strain estimation using spatio temporal elastic registration of ultrasound images: A feasibility study, Medical Imaging, IEEE Transactions on 27 (11) (2008) 1580 –1591.

[20] K. Esther Leung, M. van Stralen, A. Nemes, M. Voormolen, G. van Burken, M. Geleijnse, F. ten Cate, J. Reiber, N. de Jong, A. van der Steen, J. Bosch, Sparse registration for three-dimensional stress echocardiography, Medical Imaging, IEEE Transactions on 27 (11) (2008) 1568–1579.

[21] A. Myronenko, X. Song, D. Sahn, Maximum Likelihood Motion Estimation in 3D Echocardiography through Non-rigid Registration in Spherical Coordinates, Functional Imaging and Modeling of the Heart (2009) 427–436.

[22] D. Loeckx, P. Slagmolen, F. Maes, D. Vandermeulen, P. Suetens, Nonrigid image registration using conditional mutual information, Medical Imaging, IEEE Transactions on 29 (1) (2010) 19 –29.

[23] X. Zhuang, D. Hawkes, S. Ourselin, Unifying encoding of spatial information in mutual information for nonrigid registration, in: Information Processing in Medical Imaging, Vol. 5636 of Lecture Notes in Computer Science, Springer Berlin / Heidelberg, 2009, pp. 491–502.

[24] D. Lee, M. Hofmann, F. Steinke, Y. Altun, N. Cahill, B. Scholkopf, Learning similarity measure for multi-modal 3d image registration, in: Computer Vision and Pattern Recognition. IEEE Conference on, 2009, pp. 186 –193. doi:10.1109/CVPR.2009.5206840.

[25] M. Bronstein, A. Bronstein, F. Michel, N. Paragios, Data fusion through cross-modality metric learning using similarity-sensitive hashing, in: Computer Vision and Pattern Recognition (CVPR). IEEE Conference on, IEEE, 2010, pp. 3594–3601.

[26] P. Shankar, V. Dumane, J. Reid, V. Genis, F. Forsberg, C. Piccoli, B. Goldberg, Classification of ultrasonic b-mode images of breast masses using nakagami distribution, Ultrasonics, Ferroelectrics and Frequency Control, IEEE Transactions on 48 (2) (2002) 569–580.

[27] A. Larrue, J. A. Noble, Nakagami imaging with small windows, IEEE International Symposium on Biomedical Imaging: From Nano to Macro (2011) 887–890.

[28] N. Bouhlel, S. Sevestre-Ghalila, Nakagami markov random field as texture model for ultrasound rf envelope image, Computers in Biology and Medicine 39 (6) (2009) 535–544.

[29] T. Klein, M. Hansson, N. Navab, Spatial statistics based feature descriptor for rf ultrasound data, IEEE International Symposium on Biomedical Imaging: From Nano to Macro (2011) 33–36.

[30] C. Wachinger, T. Klein, N. Navab, The 2D Analytic Signal on RF and B-mode Ultrasound Images, in: Information Processing in Medical Imaging (IPMI), 2011, pp. 359–370.

[31] L. Wietzke, G. Sommer, O. Fleischmann, The geometry of 2d image signals, in: CVPR, 2009, pp. 1690–1697.

[32] C. Kotropoulos, X. Magnisalis, I. Pitas, M. Strintzis, Nonlinear ultrasonic image processing based on signal-adaptivefilters and self-organizing neural networks, Image Processing, IEEE Transactions on 3 (1) (1994) 65–77.

[33] P. M. Shankar, J. M. Reid, H. Ortega, C. W. Piccoli, B. B. Goldberg, Use of non-rayleigh statistics for the identification of tumors in ultrasonic b-scans of the breast, IEEE Trans. Med. Imag. 12 (4-5) (1993) 687–692.

[34] E. Jakeman, P. N. Pusey, A model for non-rayleigh sea echo, IEEE Trans. Antennas Propag. 24 (4-5) (1976) 806–814.

[35] P. Shankar, A model for ultrasonic scattering from tissues based on the k distribution, Physics in medicine and biology 40 (1995) 1633.

[36] V. Dutt, J. F. Greenleaf, Ultrasound echo envelope analysis using a homodyned k-distribution signal model, Ultrason. Imag. 16 (4-5) (1994) 265–287.

[37] T. Eltoft, The rician inverse gaussian distribution: a new model for non-rayleigh signal amplitude statistics, Image Processing, IEEE Transactions on 14 (11) (2005) 1722–1735.

[38] P. M. Shankar, A general statistical model for ultrasonic backscattering from tissues, Ultrasonics, Ferroelectrics and Frequency Control, IEEE Transactions on 47 (3) (2000) 727 –736.

[39] N. Nakagami, The m-distribution, a general formula for intensity distribution of rapid fadings, in: W. G. Hoffman (Ed.), Statistical Methods in Radio Wave Propagation, Oxford, England: Pergamon, 1960, pp. 3–36.

[40] P. Shankar, V. Dumane, J. Reid, V. Genis, F. Forsberg, C. Piccoli, B. Goldberg, Classification of ultrasonic B-mode images of breast masses using Nakagami distribution, Ultrasonics, Ferroelectrics and Frequency Control, IEEE Transactions on 48 (2) (2001) 569–580.

[41] F. Destrempes, J. Meunier, M.-F. Giroux, G. Soulez, G. Cloutier, Segmentation in ultrasonic b-mode images of healthy carotid arteries using mixtures of nakagami distributions and stochastic optimization., IEEE Trans Med Imaging 28 (2) (2009) 215–229.

[42] R. Cobbold, Foundations of biomedical ultrasound, Oxford University Press, USA, 2007.

[43] P. A. Viola, Alignment by maximization of mutual information, Ph.d. thesis, Massachusetts Institute of Technology (1995).

[44] A. Roche, G. Malandain, N. Ayache, Unifying maximum likelihood approaches in medical image registration, International Journal of Imaging Systems and Technology: Special Issue on 3D Imaging 11 (1) (2000) 71–80.

[45] A. Papoulis, U. S. Pillai, Probability, Random Variables and Stochastic Processes, McGraw-Hill; 3rd edition, 1991.

[46] C. Wachinger, N. Navab, Ultrasound specific similarity measures for three-dimensional mosaicing, in: SPIE Medical Imaging, San Diego, California, USA, 2008, p. 69140F.

[47] A. Myronenko, Non-rigid image registration: Regularization, algorithms and applications, Ph.D. thesis, Oregon Health and Science University (2010).